# Infragravity wave source regions determined from ambient noise correlation

Nicholas Harmon,[1] Timothy Henstock,[1] Meric Srokosz,[2] Frederik Tilmann,[3] Andreas Rietbrock,[4] and Penny Barton[5]

Received 23 November 2011; revised 27 January 2012; accepted 28 January 2012; published 24 February 2012.

[1] We use a backprojection method to determine dominant directions of ocean infragravity waves from 60–200 s period from cross correlations between 5 ocean bottom differential pressure gauges located off the coast of Sumatra. We observe infragravity waves arriving from all directions, but there is a dominant source direction that represents coherent propagation along the coast from the southeast or from the south. This study demonstrates the effectiveness of our projection technique, which may be applied to past and future seismic data to improve models of ocean infragravity wave generation and tsunami propagation. **Citation:** Harmon, N., T. Henstock, M. Srokosz, F. Tilmann, A. Rietbrock, and P. Barton (2012), Infragravity wave source regions determined from ambient noise correlation, *Geophys. Res. Lett.*, *39*, L04604, doi:10.1029/2011GL050414.

## 1. Introduction

[2] Ocean infragravity waves (<0.04 Hz) are generated by the interaction of higher frequency swell with coastlines [*Herbers et al.*, 1995a]. These waves are important for nearshore processes, and for the generation of the Earth's seismic 'hum' when they interact nonlinearly at continental shelves and in large ocean basins [*Rhie and Romanowicz*, 2006; *Webb*, 2007, 2008]. In the surf zone, infragravity waves are responsible for "surfbeat" and can contribute as much as 50% of the wave elevation variance [*Webb et al.*, 1991]. They can also affect nearshore sediment transport and cause harbour oscillations. The velocity of infragravity waves in deep water is generally well predicted by gravity wave theory [*Webb et al.*, 1991], but the loci of generation are unknown in remote areas.

[3] Seismic stations located on the ocean bottom with pressure records are sensitive to both seismic noise and to pressure fluctuations caused by the passage of ocean infragravity waves [*Webb*, 1998]. Ocean bottom pressure gauges and seismometers have been used previously to study ocean wave directional spectra using closely spaced arrays near shore [*Goodman et al.*, 1989; *Herbers et al.*, 1995a] and in deep water [*Webb et al.*, 1991] or by using multiple components of ground motions [*Bromirski et al.*, 2005; *Dolenc et al.*, 2008]. Here we use ambient noise correlation functions for an array of widely spaced (>30 km) ocean bottom seismometers [*Minshull et al.*, 2005] with differential pressure gauges (DPG) to monitor infragravity wave generation and propagation during the deployment period.

## 2. Methods

[4] We use ocean bottom pressure data from 9 stations deployed from June 2008 to February 2009 off the coast of Sumatra (Figure 1) as part of the UK Sumatra Consortium [*Henstock et al.*, 2010] equipped with short period geophones and differential pressure gauges. We focus on five stations located in deep water, where the infragravity wavefield has clear direct arrivals that can be effectively modelled. The stations located between Sumatra and Siberut, Nias and Batu Islands showed too much wavefield complexity to be analyzed with the methods described here.

[5] The pressure data from each station are resampled to 1 Hz, and amplitude normalized using the envelope of the data to reduce the effects of earthquakes in the data. We cross correlate all possible station pairs for each day, and generate a stack of 200 days in 2008 of the daily data for each station pair, which we refer to as the noise correlation function (NCF). The NCF for each station pair are then used to estimate the dominant source regions of infragravity waves in the region of the array.

[6] Amplitudes of the DPGs are not well calibrated and for logistical reasons we did not calibrate the instruments, so comparison of NCF between the different stations is difficult. For a given NCF, amplitude differences between the positive and negative lag indicate a difference in the amount of coherent energy propagating in either direction. By amplitude normalization and stacking as described above, we effectively "count" the number of coherent days of wave propagation across each station pair. However, for future studies, DPG sensitivity can be calibrated either *in situ* by natural sources or in the laboratory prior to deployment and true amplitude cross-correlations could be calculated instead.

[7] We use spectrograms from a two hour ($\pm 3600$ s lag) window of the NCF to examine the spectral content and apparent group arrival times. We calculate the spectrograms by using the envelope of narrow bandpass filtered time series at each frequency of interest (from 0.005–0.10 Hz w/ center frequency $\pm 0.002$ Hz), which provides signal amplitude as a function of time and frequency. The time axis is converted to the group velocity axis by dividing the lag time axis of the spectrogram into the great circle distance for the given station pair.

[1]School of Ocean and Earth Science, University of Southampton, Southampton, UK.
[2]National Oceanography Centre, Southampton, Southampton, UK.
[3]GFZ German Research Centre for Geosciences, Potsdam, Germany.
[4]Department of Earth Sciences, University of Liverpool, Liverpool, UK.
[5]Department of Earth Sciences, University of Cambridge, Cambridge, UK.


0094-8276/12/2011GL050414

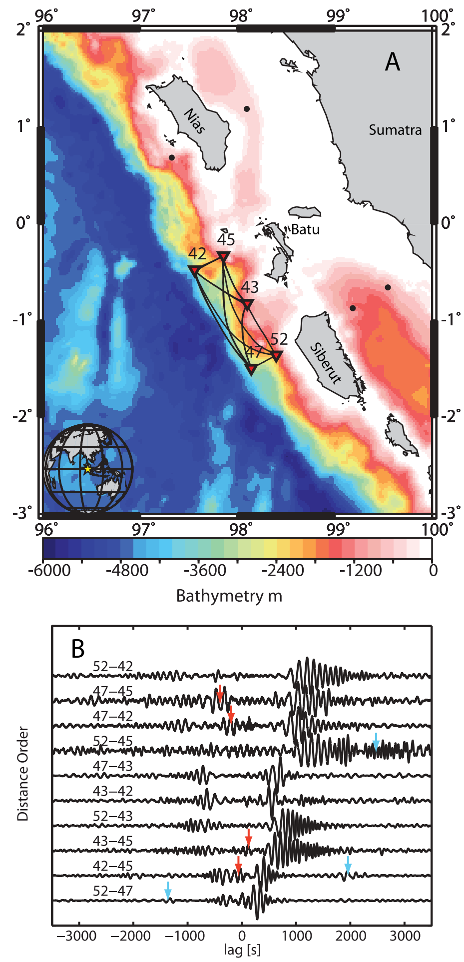


**Figure 1.** (a) Bathymetric map of study region, with station locations (red triangles, stations used, black circles, other stations deployed). Group velocity ray paths for 150 s period direct waves are shown between the stations used in the study. (b) Stacked noise correlation functions for all possible station-to-station paths. Positive lags correspond to waves propagating from station 1 to station 2 (e.g., 42–45), while negative lags are times series for waves propagating in the opposite direction. Red arrows indicate strong non-direct path early arrivals, while cyan arrows indicate reflected arrivals likely from the coast in the NCF.

[8] For comparison to our spectrograms, the theoretical group velocity (U) for each station-to-station pair is calculated based on the average water depth (H) along the great circle path between the two stations, which is a first order approximation. We use the dispersion relationship for surface gravity waves relating angular frequency, $\omega$, gravitational acceleration, g = 9.81 m/s$^2$, and wavenumber, k:

$$\omega = \sqrt{kg \tanh(kH)} \tag{1}$$

$$U = \frac{\partial \omega}{\partial k} \tag{2}$$

To model locations of sources of infragravity waves, we back project the NCF into the spatial domain. Our backprojected source density, P, is generated using the following relationship:

$$P(\phi,\theta,\omega) = \frac{1}{W(\phi,\theta,\omega)} \sum_{i}^{5} \sum_{j=i+1}^{5} env\left(R_{ij}\left(t_i(\phi,\theta,\omega) - t_j(\phi,\theta,\omega)\right)\right) \tag{3}$$

Where *env* is the envelope of the narrow bandpass filtered (center frequency, $\omega/2\pi \pm 0.002$ Hz) noise correlation function, $R_{ij}$, between the stations corresponding to indices i and j, $\phi$ and $\theta$ are latitude and longitude, W is the isotropic array response described below and $t_{i,j}$ indicates the group travel time from the source location to the station indicated by the index. The maximum value for the envelope of $R_{ij}$ is normalized to 1. The great circle path approximation is not accurate enough for the group travel time calculations, so we use a ray theoretical approach. We calculate the group

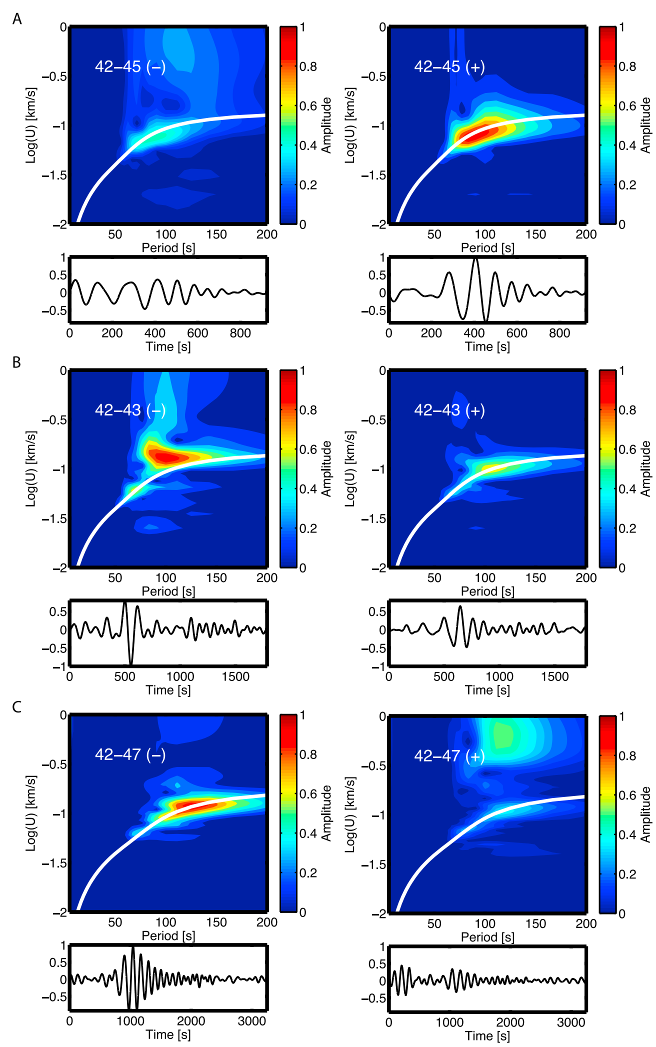


**Figure 2.** Spectrograms of normalized time series shown in Figure 1b for (a) 42–45, (b) 42–43 and (c) 42–47, with (left) positive lags and (right) negative lags. Corresponding time series are shown beneath the spectrograms. White lines in spectrograms indicate predicted group dispersion based on the average water depth/great circle path assumption using equations (1) and (2).

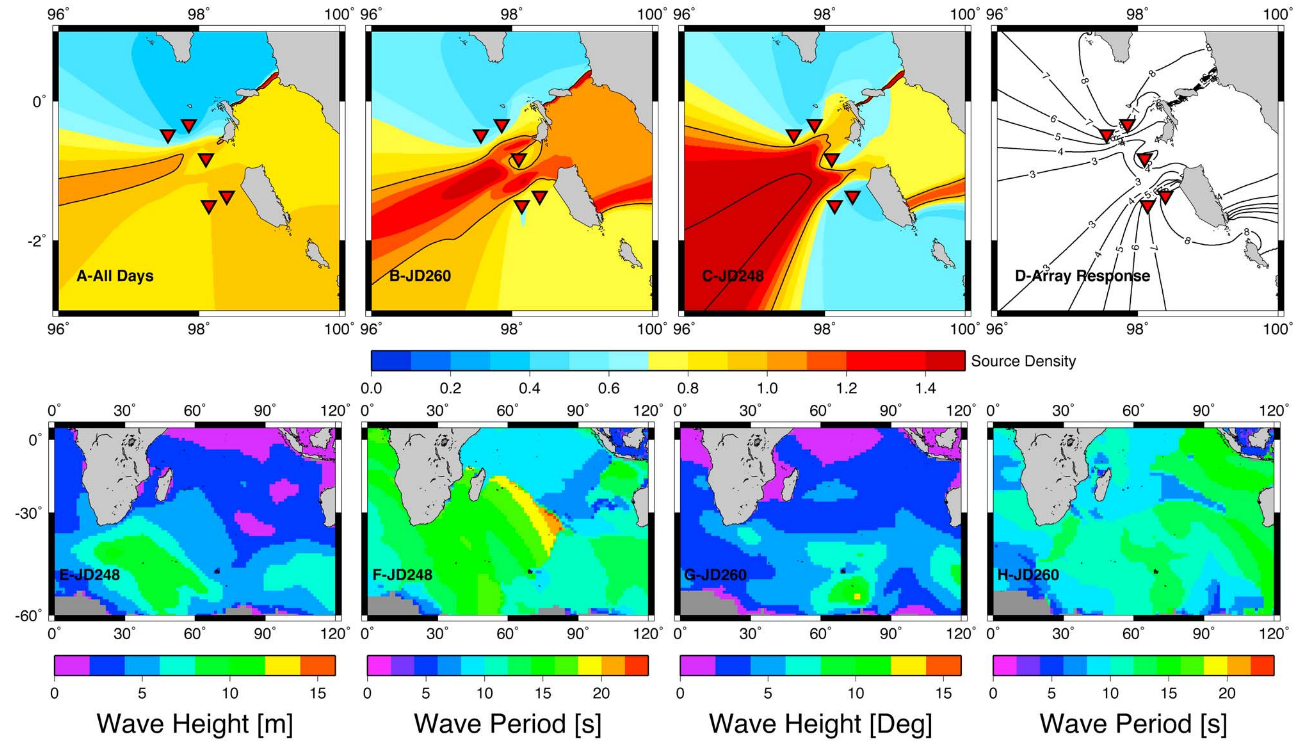


**Figure 3.** Source density from projection of the envelope of the NCF at 150 s period, for (a) all days stacked, (b) September 16, 2008 (JD = 260) and (c) September 4, 2008 (JD = 248). (d) Isotropic source response of the array. Greater source densities indicate more likely regions of infragravity wave sources. (e) Wave height, (f) dominant wave period for Sept. 4, 2008 and (g) wave height, (h) dominant wave period for Sept. 16, 2008 from WAVEWATCH III hindcast [*NOAA*, 2011] models.

velocity map for the area for a given $\omega$ using equations (1) and (2), with satellite derived bathymetry [*Smith and Sandwell*, 1997] for H. We calculate group travel times for a source at each station location to each point (on a 1 minute grid) in the map by solving the Eikonal wave equation using a finite difference algorithm [*Rawlinson and Sambridge*, 2004], which calculates the minimum direct travel time. This method is similar to other projection methods used to study ambient seismic noise [*Brzak et al.*, 2009; *Rhie and Romanowicz*, 2006].

[9] We calculate the isotropic response of our projection method assuming an isotropic distribution of plane waves, which yields a theoretical correlation function, $R_{ij}$, at lag time t, $R(t) = 1/\pi\sqrt{(t_U^2 - t^2)}$ for each station-to-station pair [*Aki*, 1957; *Harmon et al.*, 2008]. We determine $t_U$, the group arrival time of a direct wave arrival along the station-to-station ray path, from our ray theoretical calculations. We then apply a narrow band pass filter centered on the frequency of interest ($\pm$0.002 Hz), and calculate the envelope of the function. The theoretical correlation function produced group arrival times that were within 10–60 s of the observed group arrival times at 150 s period. We then use equation (3) to project the synthetic data to generate the isotropic response assuming W is 1.

## 3. Results

[10] The noise correlation functions in Figure 1b show strong arrivals at both positive and negative time lags; the arrivals are visibly dispersed, with lower frequency arrivals at time lags closer to zero. Although energy is seen coming from all directions sampled by our array, the amplitudes of the main direct arrivals are asymmetric for all of the station-to-station pairs indicating there is a preferred direction of propagation. In addition, smaller arrivals are visible in noise correlation functions before and after the main arrivals in the noise correlations.

[11] The spectrograms (Figures 2a–2c) show the apparent group velocity of the main arrivals visible in Figure 1b. There is a clear pattern of dispersion visible for most station-to-station paths at both positive and negative time lags from $\sim$60–200 s period from 50–200 m/s group velocity, with longer periods having greater velocities. In addition, there are non-direct path (early) arrivals in either the positive or negative lags at faster (>200 m/s) velocities (e.g., 42–47) corresponding to energy propagating obliquely with respect to the direct path.

[12] Our estimates of the location of the sources of infragravity waves for 150 s period from backprojecting the NCF energy shown in Figures 3a–3c are shown with the isotropic source response of our array geometry in Figure 3d. Likely source locations are to the south and southeast along the coast of Siberut Island for the 200 day stack (Figure 3a), and a similar pattern for Sept. 16, 2008 (Figure 3b). There is also a strong arrival visible from the west-southwest seen in Figures 3b and 3a. In general, we observe much less energy in the northern part of the study area.

[13] However, a notable exception to the patterns observed in Figures 3a and 3b is from Sept. 2, 2008–Sept. 6, 2008 (JD 246-50); illustrated in Figure 3c for Sept. 4, 2008. During this time the source direction is dominantly from the south-west. The largest amplitudes for station-to-station path 47–52

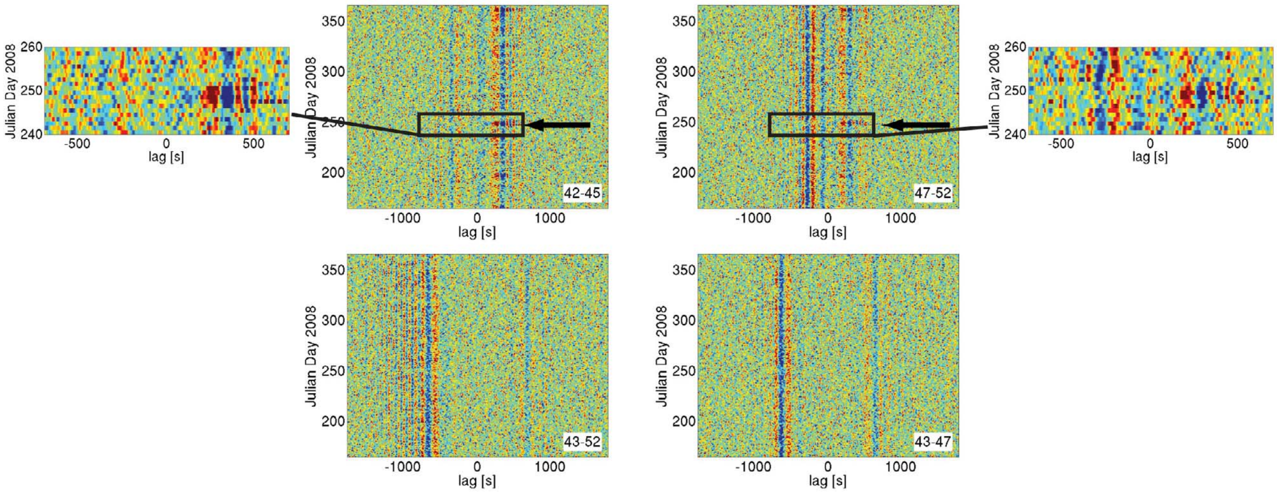


**Figure 4.** Noise correlation functions as a function of Julian Day 2008 for 42–45, 47–52, 43–52, and 43–47. Color scale is constant across panels and saturates at ±0.5. Black arrows indicate the event on Sept. 2–6, 2008 (JD 246-250), expanded views are provided as outset panels.

are found at positive lags (Figure 4), switching the sense of onshore-offshore infragravity wave propagation for this station-to-station path. Also during this time, in the along shore direction, the NCF for 43–52 exhibits a marked decrease in coherency (Figure 4).

[14] Otherwise, there is little variation through time in the relative energy in the noise correlation functions between positive and negative lags for select station pairs (Figure 4) and the sense of infragravity propagation across the array is thus relatively stable during the time period of our study. For example, during the time period of our study, station-to-station path 42–45 has higher energy on the positive time lags while 47–52 has consistently higher energy on the negative lags than the positive lag, suggesting an opposite sense of infragravity wave propagation onshore-offshore between the northern and southern part of the array. Therefore, overall infragravity wave generation is relatively constant.

## 4. Discussion

[15] Comparison with the predicted group velocities for the great circle path (white solid line in Figure 2) shows good agreement with the dispersion in the spectrograms for both positive and negative lags in most cases, and differences can be attributed to the break down of the great circle path approximation known from ray tracing (ray paths for direct wave at 150 s shown in Figure 1a) and errors associated with the average depth assumption. As suggested by *Webb et al.* [1991] the agreement with the predicted dispersion relationship indicates the infragravity waves traveling across the array are free waves at the surface. The presence of coherent energy at both positive and negative lags suggest that the wavefield in the region has some energy in all directions, which is also consistent with free waves [*Herbers et al.*, 1995a].

[16] The source densities shown in Figures 3a and 3b suggest the dominant source region for the infragravity waves is from the south from the Indian Ocean, or from waves generated and refracted along the coast by the bathymetry. The coherent source region visible in Figures 3a and 3b coming from the west-southwest, near the Batu islands appears to suggest that there may be either infragravity wave generation on the shallow coasts of the islands or scattering of the wave field propagating along the coast. This energy is generated from projecting the non-direct (early) arrivals visible in Figure 1b for 42–43, and 43–45 and the direct arrival from 42–45. As the isotropic response (Figure 3d) shows low sensitivity in the region, this peak in the observed distribution cannot be interpreted with certainty. Based on comparison with the array response for isotropic sources generated outside the array (Figure 3d), our resolution is limited, with greater sensitivity (strong lobes) to sources coming from the coasts. The presence of non-direct path (early) arrivals in many of the NCF suggests some energy propagating in a direction oblique to the coast or refracting out into deeper water, and the coherent later arrivals after the main arrival suggest there are significant reflections from the coastline but are difficult to interpret in detail. The source regions of infragravity waves also appear to be very consistent throughout most of the study period. However, our array geometry and amplitude normalization, make it difficult to identify individual events coming from the southern Indian Ocean.

[17] The change in dominant direction of the infragravity wave source region on JD 246–250 (Figures 4 and 3c) likely corresponds to a the arrival of trans-Indian Ocean infragravity waves generated by coastal interactions of waves from a storm on Sept. 1, 2008 off the southern tip of Africa, ~8800 km away as seen in NOAA WAVEWATCH III hindcasts [*NOAA*, 2011; *Tolman*, 2005]. The arrival time and source direction are consistent with a storm located in this region. Global NOAA WAVEWATCH III hindcasts [*NOAA*, 2011; *Tolman*, 2005] show this storm generated very long dominant period (20–25 s) gravity waves for several days and >10 m wave heights, which then took 6 days to propagate across the Indian Ocean with a group velocity of ~0.015 km/s with a wave direction ~225° azimuth (Sept. 4, 2008 shown Figures 3e and 3f, and for comparison Sept. 16, 2008 in Figures 3g and 3h). The wave action models do not generate waves in the infragravity period range, but we infer that the development of 25 s dominant period in the

model may indicate transfer of energy to even longer periods. As noted by *Webb et al.* [1991] and *Herbers et al.* [1995b], near the coast nonlinear wave-wave interactions transfer energy from gravity waves to free infragravity waves, which then can propagate across the ocean. The arrival of the observed long period (~150–200 s) infragravity waves took ~1 day and had an azimuth of ~200–250°, which suggests a group velocity of ~0.10–0.15 km/s, which is in good agreement with deep-water group propagation and generation at the southern tip of Africa.

## 5. Conclusions

[18] We have shown that noise correlation of DPG data shows coherent energy related to ocean gravity waves between the station-to-station pairs, which can be used to infer group dispersion between them. The records can also be used to infer dominant directions of wave propagation. In our study region, we find a dominant region for coherent infra gravity wave generation in the south and/or along the coast of Sumatra based on projection of normalized noise correlation functions. We also find significant contributions from storm-generated infragravity waves propagating from the southwest. Past and future seismic data sets may be used to improve models of ocean infragravity wave generation and tsunami propagation (see *Webb et al.* [1991], on relationship to tsunamis) by providing better constraints in remote regions without buoy data.

[19] **Acknowledgments.** This work was supported by the United Kingdom's Natural Environment Research Council grant NE/D004381/1, and the Ocean Bottom Instrument Facility provided the data. We also thank Spahr Webb and an anonymous reviewer for their constructive comments.

[20] The Editor thanks Spahr Webb and an anonymous reviewer for their assistance in evaluating this paper.

## References

Aki, K. (1957), Space and time spectra of stationary and stochastic waves, with special reference to microtremors, *Bull. Earthquake Res. Inst. Univ. Tokyo*, *35*, 415–457.

Bromirski, P. D., F. K. Duennebier, and R. A. Stephen (2005), Mid-ocean microseisms, *Geochem. Geophys. Geosyst.*, *6*, Q04009, doi:10.1029/2004GC000768.

Brzak, K., Y. J. Gu, A. Ökeler, M. Steckler, and A. Lerner-Lam (2009), Migration imaging and forward modeling of microseismic noise sources near southern Italy, *Geochem. Geophys. Geosyst.*, *10*, Q01012, doi:10.1029/2008GC002234.

Dolenc, D., B. Romanowicz, P. McGill, and W. Wilcock (2008), Observations of infragravity waves at the ocean-bottom broadband seismic stations Endeavour (KEBB) and Explorer (KXBB), *Geochem. Geophys. Geosyst.*, *9*, Q05007, doi:10.1029/2008GC001942.

Goodman, D., et al. (1989), Directional spectra observations of seafloor microseisms from an ocean-bottom seismometer array, *J. Acoust Soc. Am.*, *86*(6), 2309–2317, doi:10.1121/1.398438.

Harmon, N., P. Gerstoft, C. A. Rychert, G. A. Abers, M. Salas de la Cruz, and K. M. Fischer (2008), Phase velocities from seismic noise using beamforming and cross correlation in Costa Rica and Nicaragua, *Geophys. Res. Lett.*, *35*, L19303, doi:10.1029/2008GL035387.

Henstock, T., et al. (2010), Exploring structural controls on Sumatran earthquakes, *Eos Trans. AGU*, *91*(44), 405, doi:10.1029/2010EO440002.

Herbers, T. H. C., S. Elgar, and R. T. Guza (1995a), Generation and propagation of infragravity waves, *J. Geophys. Res.*, *100*(C12), 24,863–24,872, doi:10.1029/95JC02680.

Herbers, T. H. C., et al. (1995b), Infragravity-frequency (0.005–0.05 Hz) motions on the shelf. 2. Free waves, *J. Phys. Oceanogr.*, *25*(6), 1063–1079, doi:10.1175/1520-0485(1995)025<1063:IFHMOT>2.0.CO;2.

Minshull, T. A., et al. (2005), Multi-disciplinary, sub-seabed geophysical imaging, *Sea Technol.*, *48*(10), 27–31.

NOAA (2011), NOAA WaveWatch III model output archive, ftp://polar.ncep.noaa.gov/pub/history/waves/, Camp Springs, Md.

Rawlinson, N., and M. Sambridge (2004), Wave front evolution in strongly heterogeneous layered media using the fast marching method, *Geophys. J. Int.*, *156*(3), 631–647, doi:10.1111/j.1365-246X.2004.02153.x.

Rhie, J., and B. Romanowicz (2006), A study of the relation between ocean storms and the earth's hum, *Geochem. Geophys. Geosyst.*, *7*, Q10004, doi:10.1029/2006GC001274.

Smith, W. H. F., and D. T. Sandwell (1997), Global seafloor topography from satellite altimetry and ship soundings, *Science*, *277*, 1956–1962, doi:10.1126/science.277.5334.1956.

Tolman, H. L. (2005), *Manual and Wave User System Documentation of WAVEWATCH III*, NOAA, Camp Springs, Md.

Webb, S. C. (1998), Broadband seismology and noise under the ocean, *Rev. Geophys.*, *36*(1), 105–142, doi:10.1029/97RG02287.

Webb, S. C. (2007), The Earth's 'hum' is driven by ocean waves over the continental shelves, *Nature*, *445*(7129), 754–756, doi:10.1038/nature05536.

Webb, S. C. (2008), The Earth's hum: The excitation of Earth normal modes by ocean waves, *Geophys. J. Int.*, *174*(2), 542–566, doi:10.1111/j.1365-246X.2008.03801.x.

Webb, S. C., X. Zhang, and W. Crawford (1991), Infragravity waves in the deep ocean, *J. Geophys. Res.*, *96*(C2), 2723–2736, doi:10.1029/90JC02212.

P. Barton, Department of Earth Sciences, University of Cambridge, Madingley Road, Cambridge CB3 0EZ, UK.

N. Harmon and T. Henstock, School of Ocean and Earth Science, University of Southampton, European Way, Southampton SO14 3ZH, UK. (n.harmon@soton.ac.uk)

A. Rietbrock, Department of Earth Sciences, University of Liverpool, 4 Brownlow St., Liverpool L69 3GP, UK.

M. Srokosz, National Oceanography Centre, Southampton, European Way, Southampton SO14 3ZH, UK.

F. Tilmann, GFZ German Research Centre for Geosciences, Telegrafenberg, D-14473 Potsdam, Germany.